Check for updates

Chitosan nanobeads loaded with Biginelli hybrids as cell-selective toxicity systems with a homogeneous distribution of the cell cycle in cancer treatment†

Jovana Ristovski (Trifunović),[a] Željko Žižak,[b] Smilja Marković,[c] Nenad Janković [ID] *[d] and Nenad Ignjatović [ID] *[c]

Tetrahydropyrimidines are a class of azaheterocycles, also called Biginelli hybrids (obtained from the Biginelli reaction), that have attracted an enormous interest in the medicinal chemistry community in recent years, due to a broad biological activity, such as anticancer, antiviral, anti-inflammatory, antidiabetic, antituberculosis activities, *etc.* According to SciFinder®, more than 70 000 different Biginelli-like compounds have been covered in publications. However, although the Biginelli reaction can yield a large number of compounds with a broad range of activities, none of them have been captured in a carrier. In this study, chitosan-based (Ch) nanoparticles (NPs) containing three different molecules (Biginelli hybrids) were developed and tested for the first time as simple and promising vehicles for anticancer Biginelli-based drugs. The key features of NPs, such as size, surface morphology, drug encapsulation efficiency, and *in vitro* release were systematically investigated. Rather weak cell selectivity of pure Biginelli hybrids (**A–C**) to selected cancer cell lines has improved and this has been accompanied with two-to-four times stronger cytotoxic effect of **A–C** loaded Ch NPs, with a triple reduction in toxicity to healthy cells (MRC-5). It has been observed that the examined NPs induce apoptosis. The cell cycle analysis has confirmed the influence of **A**-loaded Ch (**A-Ch**), **B**-loaded Ch (**B-Ch**), and **C**-loaded Ch (**C-Ch**) on the cell cycle distribution, which was homogenously affected. This is the difference with regard to the effect of **A**, **B**, and **C** on the cell cycle. It has been established that the increased selectivity and antitumor activity of NPs are related to the presence of the carrier.

Introduction

The Biginelli reaction was developed by Pietro Biginelli in 1893. In this acid-catalysed one-pot synthesis, aldehyde, β-ketoester and urea(thiourea) participate in the development of tetrahydrpyrimidines-THPMs (formerly known as 3,4-dihydropyrimidin-2(1*H*)-ones). This class of compounds are particularly interesting in pharmaceutical sciences due to the biological activity associated with their heterocyclic structure. THPMs have been used therapeutically as calcium channel modulators (*e.g.* nifedipine, nicardipine and amlodipine), as

well as α1-adrenergic receptor antagonists (*e.g.* terazosin and niguldipine).[1–3] The anticancer activity of THPMs is based on their ability to interrupt the cell cycle during mitosis. The molecules that perturb microtubule depolymerization or polymerization block the cell cycle in mitosis by disturbing the normal microtubule dynamics. Several drugs that bind to tubulin and inhibit spindle assembly may be cited as examples, *e.g.* paclitaxel and docetaxel, as well as vinca and colchicine analogues. The first THPM identified as a mitotic kinesin inhibitor was monastrol, in 1999. Since then, many THPMs have been synthesized and tested as potential Eg5 inhibitors.[3,4]

Despite the apparent advances in therapy development over the last decades, cancer is still the second leading cause of death globally. With millions of deaths each year, lung, prostate, colorectal, stomach and liver cancer are the most common types of cancer in men, while breast, colorectal, lung, cervical and thyroid cancer are the most represented among women. Cancer therapy nowadays includes several different approaches, including surgery, chemotherapy, radiation therapy, immunotherapy, and targeted therapy. It is very common that different approaches are combined to achieve the best therapeutic

[a]Department of Pharmacology, Toxicology and Clinical Pharmacology, Faculty of Medicine, University of Novi Sad, Serbia

[b]Institute of Oncology and Radiology of Serbia, Pasterova 14, 11000, Belgrade, Serbia

[c]Institute of Technical Sciences of the Serbian Academy of Science and Arts, Knez Mihailova 35/IV, P.O. Box 377, 11000, Belgrade, Serbia. E-mail: nenad.jankovic@kg.ac.rs; nenad.ignjatovic@itn.sanu.ac.rs

[d]Institute for Information Technologies Kragujevac, Department of Science, University of Kragujevac, Jovana Cvijića bb, 34000 Kragujevac, Serbia

† Electronic supplementary information (ESI) available. See DOI: 10.1039/d0ra08085c

outcome. Many cancer types are usually associated with reduced long-term survival and an unsatisfactory quality of life. However, a sufficiently effective therapy has not yet been developed and innovative drug delivery is considered as one of the ways to improve the existing therapy.[5–8]

Recent decades have witnessed an exceptional growth of research in nanotechnology. Nanoparticles (NPs) are widely studied products in medicine due to their nanoscale sizes and comparatively large surfaces, as well as their capacity to interact with different biological systems more efficiently with a better therapeutic outcome. Also, due to their ability to adsorb and carry other molecules, they are relevant for the transport and release of different drugs, probes, and proteins. One of the main issues in nanotechnology is to select appropriate carriers meeting specific requirements regarding incorporation and release, stability, biocompatibility, biodistribution, and possible adverse effects.[9–13]

Biodegradable polymers are very suitable for drug formulations as they do not require any elimination pathway from human body. One of the most used materials for this purpose is chitosan (Ch). Its biocompatibility and mechanical properties make it a very convenient candidate for nanoformulations. Ch is a polysaccharide consisting of glucosamine and N-acetylglucosamine units. The protonation of amine groups in glucosamine units requires slightly acidic pH. As a result, the whole molecule has cationic properties, enabling interactions with different anionic structures, such as cell membranes, nucleic acids, and macromolecules. Drug release from Ch-based systems primarily depends on the physicochemical characteristics of the incorporated drugs. The mechanisms that could be involved in drug release of Ch-based dosage forms include: (1) diffusion, (2) swelling, (3) erosion and (4) biodegradation. In recent years, Ch has been extensively exploited as a cationic polymer material in the delivery of anticancer drugs. Fast degradation and intensive swelling in aqueous solutions could lead to rapid drug release. Consequently, in the development of sustained drug release systems, physical and chemical modifications of chitosan are required in order to improve the stability of formulations in neutral or alkaline environments.[14–17]

Our previous research, highlights that anticancer drugs based on anticancer compounds loaded into nanoparticles of bioresorbable polymers have improved features.[18–20] With an improved understanding of nanomaterials and the application of nanotechnology our strategies are currently being directed towards improving the ability of anticancer nanostructures to target specific tissues and to reduce the toxicity of pure compounds by coating them with appropriate nanocarriers. According to SciFinder®, in July 2020, more than 70 000 different Biginelli-like compounds have been published. So far, many potential Biginelli-based drugs have failed in clinical trials due to poor water solubility and, consequently, poor bioavailability, the lack of selectivity, toxicity, and stability under physiological conditions. However, although the Biginelli reaction yields a huge number of compounds with a broad range of activities, none of them were captured in a carrier. Given the above considerations, our combined interest in sustainable, green and Biginelli chemistry,[21–27] has inspired us

to develop specific sustainable formulations with fast delivery and improved cytotoxic selectivity of the selected Bignelli hybrids in targeting cancer cell lines.

In this research, we have investigated for the first time spherical nanoparticles made of Ch and loaded with three different THPMs (Scheme 1 and Fig. 1): ethyl 6-(chloromethyl)-4-(4-hydroxy-3-methoxyphenyl)-1-methyl-2-oxo-1,2,3,4-tetrahydropyrimidine-5-carboxylate (**A**), ethyl 4-[4-(benzyloxy)phenyl]-6-(chloromethyl)-1-methyl-2-oxo-1,2,3,4-tetrahydropyrimidine-5-carboxylate (**B**) and ethyl 6-(chloromethyl)-4-(4-hydroxy-3-iodo-5-methoxyphenyl)-1-methyl-2-oxo-1,2,3,4-tetrahydropyrimidine-5-carboxylate (**C**).

As shown in Fig. 1, the difference between **A**, **B** and **C** can be observed at the C-4 position in the THPM scaffold which consists of the following aryl substituents: 4′-hydroxy-3′-methoxyphenyl (**A**), 4′-benzyloxyphenyl (**B**), and 4′-hydroxy-3′-iodo-5′-methoxyphenyl (**C**). The chemical structure of **A**, **B** and **C** is confirmed by ^{1}H and ^{13}C NMR spectra (ESI, Fig. S1–S6†). The content of compounds in chitosan nanoparticles (Ch NPs) was measured using HPLC.

Attenuated total reflectance Fourier transform infrared (ATR-FTIR) spectroscopy was applied to measure surface properties. Compound loading process was monitored by simultaneous thermogravimetric/differential thermal analyses (TGA/DTA), while scanning electron microscopy (SEM) was employed in the analysis of the morphology of NPs. Drug release tests were performed using high performance liquid chromatography (HPLC) to measure the rate of **A**, **B** and **C** release from NPs. The selective viability effect of the THP derivatives and the obtained NPs was examined using MTT assays on the four different cell lines: cervical cancer cells (HeLa), colorectal adenocarcinoma, (LS-174), human lung carcinoma (A549) and human lung fibroblasts (MRC-5). Flow cytometry was used for assessing the cell cycle, to measure cellular DNA content.

Results and discussion

In this study, free **A**, **B** and **C** Biginelli derivatives were encapsulated for the first time into the framework of Ch according to the described method. The encapsulation process was confirmed by FTIR. Fig. 2 shows the FTIR spectra of Ch, THPMs (**A**, **B** and **C**) and their appropriate nanoparticulate derivatives (**A**-loaded Ch, **B**-loaded Ch and **C**-loaded Ch) in the frequency
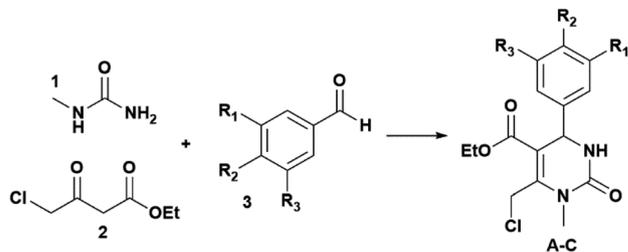
Scheme 1 Synthetic route towards THPMs (**A–C**); **A**: R_1 = OMe, R_2 = OH, R_3 = H; **B**: R_1 = R_3 = H, R_2 = PhCH$_2$O, and **C**: R_1 = OMe, R_2 = OH, R_3 = I.
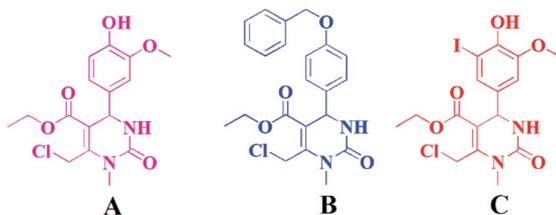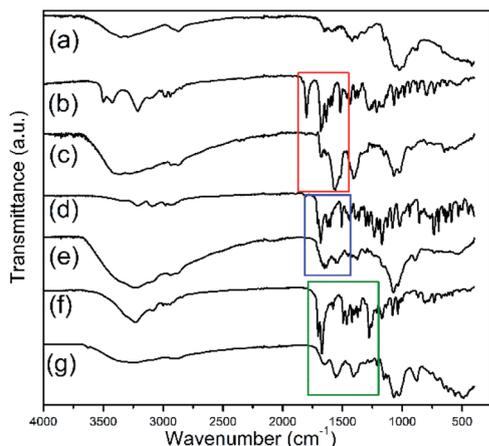
Fig. 1 Structures of Biginelli hybrids A–C.

Fig. 2 FTIR spectra of (a) Ch, (b) A, (c) A-Ch, (d) B, (e) B-Ch, (f) C and (g) C-Ch.

range from 4000 to 400 cm^{-1}. The FTIR spectra of the pure Biginelli hybrids **A**, **B** and **C** (Fig. 2b, d and f) show peaks near at: 3300 cm^{-1} – assigned to the N–H stretching vibrations, 3200 cm^{-1} – due to the C–H stretching vibrations, 1628 cm^{-1} – due to the C–N stretching vibrations, 1070 cm^{-1} – attributed to the C–O–C stretching vibrations, and 936 cm^{-1} – due to the C–H deformation. The sharp band between 1700 and 1600 cm^{-1} in the spectra of derivative **A**, **B** and **C**, originates from the vibration of the carbonyl group. This characteristic band is also present in the FTIR spectra of the **A**-loaded Ch (**A**-Ch), **B**-loaded Ch (**B**-Ch) and **C**-loaded Ch (**C**-Ch) samples (Fig. 2c, e and g).

In the FTIR spectrum of Ch, characteristic absorption bands appear at 1655 cm^{-1}, which can be attributed to both the C=O stretching vibrations and an amide I band, and at 1580 cm^{-1}, attributed to amide II band. The bands near 1066 cm^{-1} and 1028 cm^{-1} correspond to the C–O stretching vibrations. All bands are also found in the chitosan spectra reported by others.[19,28] The appearance of bands characteristic for pure Biginelli derivatives **A**, **B** and **C** in the spectra of the **A**-Ch and **B**-Ch and **C**-Ch systems may be indicative of Biginelli pyrimidines entrapped in Ch during the synthesis of NPs. Furthermore, an increased intensity of the C–H band near 3200 cm^{-1} in the spectra of the **A**-Ch, **B**-Ch and **C**-Ch systems as compared to the spectra of pure **A**, **B** and **C**, respectively, is probably due to hydrogen bonding between **A**, **B** and **C** Biginelli derivatives and Ch.

Thermogravimetric analysis (TGA) is applied to determine the mass loss of the sample over time according to temperature

changes. TGA and DTA are suitable methods for analyzing and identifying the chemical composition of nanomaterials by investigating the thermal performance of a substance as it is heated.[29]

The TGA and DTA of Ch, **A**, **A**-Ch, **B**, **B**-Ch, **C**, and **C**-Ch in the 30–700 °C temperature range are shown in Fig. 3. A moderate weight loss in Ch (Fig. 3a) at about 250 °C is associated with the loss of adsorbed water. This phenomenon is confirmed by a broad endothermic peak of the DTA curve at 100 °C (Fig. 3a). In the 250–700 °C interval, the region extending from 250 °C to 300 °C stands out with a drastic weight decrease: from 88% to 58%. It is followed by the region from 300 °C to 630 °C, where weight loss ranging from 58% to 2% is observed. The thermal degradation of chitosan is a two-step process entailed by chain scission and depolymerization reactions,[30] which could also be confirmed by the double wide exothermic peak with peaks at 300 and 482 °C. The DTA curve of compound **A** (Fig. 3b) shows two endothermic peaks, at 120 °C and 165 °C, due to water loss and melting, respectively, while a wide exothermic peak in the 200–600 °C range, with the maximum at 483 °C, probably originated from the thermal decomposition of compound **A**.

The total weight loss (100%) of compound **A** was observed at 581 °C. As it can be seen in Fig. 3c, the DTA curve of **A**-loaded Ch is dominated by peaks characteristic for compound **A** and Ch. As opposed to the DTA curve of compound **A**, the thermal decomposition of compound **B** was characterized by broad exothermic peaks with a maximum at 474 °C (Fig. 3c). The complete decomposition of compound **B** (total weight loss, 100% at 610 °C) is marked by broad exothermic peaks of the DTA curve (Fig. 3d) with a maximum at 546 °C. A broad
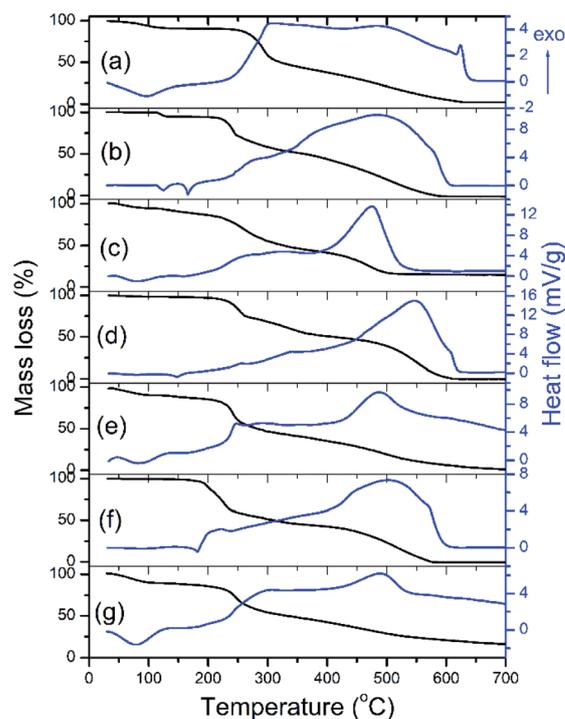

Fig. 3 TGA/DTA of (a) Ch, (b) A, (c) A-Ch, (d) B, (e) B-Ch, (f) C and (g) C-Ch.

exothermic peak with a maximum at 486 °C (Fig. 3e) is characteristic of the thermal decomposition of **B**-loaded Ch. Compound **C** decomposes completely at 576 °C (Fig. 3f) with a characteristic exothermic maximum of the DTA curves at 503 °C. The presented DTA curve of **C**-loaded Ch (Fig. 3g) is marked by a broad endothermic peak at 488 °C.

Based on the results shown in Fig. 3, it is possible to observe shifts between the maxima in the DTA curves of pure compounds **A**, **B**, **C** and compound-loaded Ch (Fig. 3b–g). These shifts are the evidence of a compound–chitosan interaction, which is most likely due to hydrogen bonding between Ch and compound. In general, a drug–chitosan interaction in drug-loaded chitosan particles results in a shift of the maximum or minimum in the DTA and DSC curves.[31,32]

SEM is routinely applied to generate high-resolution images of the morphology of different materials. In nanotechnology, it has been employed to resolve important questions regarding particle size, shape, chemical composition, crystalline structure and texture. The morphology of **A**-Ch, **B**-Ch and **C**-Ch powders is shown in Fig. 4. The encapsulation of **A**, **B** and **C** into Ch leads to the formation of particles with a spherical morphology. After the synthesis of **A**-Ch, **B**-Ch and **C**-Ch (experimental section), the particles were processed in a centrifugal field (21 000 rpm), implying that spherical morphologies were expected. In our previous research, processing in the strong centrifugal field also caused the formation of spherical morphology of polymer particles.[33] The obtained particles were not agglomerated; however, particle size distributions were not uniform. The morphological analysis reveals two size distributions in all particle types: larger particles with an average diameter of 100 ± 20 nm and smaller ones with an average diameter of 30 ± 10 nm. The possibility of obtaining bimodal profiles of particle size distributions after using emulsification–evaporation method has been highlighted in the literature.[34–36] Homogeneous and heterogeneous binary colloidal clusters can be formed by self-assembly evaporation within droplets.[34] During emulsification and high energy mixing at 21 000 rpm, the self-assembly of Biginelli compounds is possible, which leads to the formation of two size distributions.

To gain deeper insights into bioavailability and to measure drug release kinetics, measurements using HPLC were performed. The areas of released compounds (**A** retention time of 22.5 min; **B** retention time of 41.6 min and **C** retention time of 32.4 min) in HPLC chromatograms were compared and the concentrations of the released compounds were calculated.

The results are presented in the form of a cumulative curve in Fig. 5. Over 50% of pure compounds were released in the first
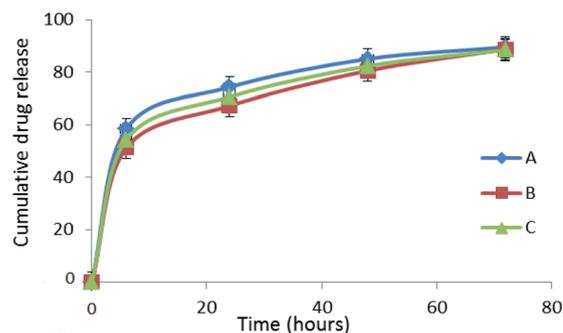
Fig. 5 Comparative cumulative curves of the release of A, B and C in percentages in PBS at 37 °C during 72 h.

6 h; in 48 h around 80% were released. Keeping in mind that Ch with a medium molecular weight was used as the carrier in the formulations, these findings are not surprising. Moreover, the complete release of the Biginelli hybrids was observed after the third day, *i.e.* 8.5%; 88.7% and 88.45% of **A**, **B** and **C** respectively. Drug encapsulation efficiency was also measured using the HPLC technique. It was confirmed that encapsulation efficiency was 90%. The ratio of Biginelli hybrids and chitosan was 20 : 80, since the efficiency was 90%, the share of entrapped **A**, **B**, and **C** was 18 wt%.

In addition, to estimate the amount of the drug (**A**, **B** or **C**) present on the surface of the NPs, detected based on the immediate release after dissolution in appropriate media, a Loose Surface Crystal Study was performed. The experimental data confirm that compounds **A**, **B** and **C** are present on the surface of NPs in concentrations smaller than 5%. Also, the drug entrapment efficiency study shows that in the first 24 h 72.32%, 70.4% and 71.2% of **A**, **B** and **C** respectively were released (Table 1).

Table 2 shows the cytotoxic values of pure derivatives **A**, **B**, **C** and their NPs on selected cell lines: cervix adenocarcinoma (HeLa), human colorectal adenocarcinoma, (LS-174), lung cancer cells (A549) and human fibroblasts (MRC-5). It has been observed that for tumor cells IC_{50}, the values for pure derivatives **A**, **B** and **C** are higher or, in some cases, practically the same as those for the corresponding NPs derivatives (**A**-Ch, **B**-Ch, and **C**-Ch). Ch is a biologically inert material, and it does not exhibit cytotoxic effects. Therefore, it can be concluded that higher cytotoxicity values can only be a consequence of the action of NPs. There are numerous examples demonstrating how different technological operations can change the effects of active pharmaceutical ingredients in appropriate drugs.[18–20] In

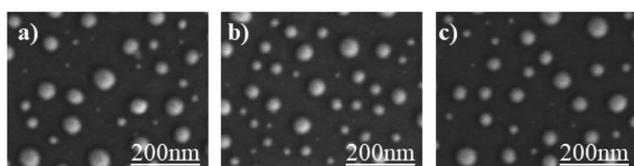Fig. 4 SEM micrographs of (a) A-Ch, (b) B-Ch, and (c) C-Ch.

Table 1 Results of loose surface and drug entrapment efficiency studies

Formulation	% DEE	% LSC
A	72.32	3.05
B	70.4	4.7
C	71.2	3.8

Table 2 Concentrations of investigated pure derivatives **A**, **B**, **C** and their NPs inducing 50% decrease (IC_{50}) in malignant and normal cell survival

IC_{50} [μg mL^{-1}] ± SD^a				
	HeLa	A549	LS174	MRC-5
Ch carrier	882 ± 14	nd	nd	830 ± 30
A-Ch	2.92 ± 0.21	5.28 ± 0.01	4.3 ± 0.02	3.70 ± 0.75
B-Ch	5.97 ± 0.14	5.76 ± 0.25	5.86 ± 0.01	8.90 ± 0.14
C-Ch	5.61 ± 0.13	5.94 ± 0.05	5.78 ± 0.18	11.74 ± 0.13
A	9.53 ± 0.15	10.42 ± 0.92	10.31 ± 0.54	4.3 ± 0.10
B	5.00 ± 0.30	6.72 ± 0.32	7.12 ± 0.36	3.22 ± 0.05
C	5.05 ± 0.21	8.39 ± 0.02	4.71 ± 0.12	2.56 ± 0.03

^{a} From three independent experiments.

this case, the incorporation of **A**, **B** and **C** in NPs resulted not only in greater cytotoxicity but also in greater selectivity in action toward tumor than normal cells. In the MRC-5 cell line, which is a healthy human cell line, it has been observed that stronger cytotoxic effects are caused by pure hybrids than by appropriate NPs. Only in case of pure hybrid **A**, the IC_{50} value is higher than that in the corresponding NPs system (**A**-Ch).

Apoptosis is a form of programmed cell death regulated by specific genes and it has a role in the elimination of physiologically redundant, physically damaged, and abnormal cells. By employing acridine orange/ethidium bromide fluorescent staining, it is possible to detect apoptosis-associated changes of cellular nuclei.

Fig. 6 shows the results of experiments without the NPs and after the treatment with the selected NPs. In the control group, no significant apoptosis was detected, but cells in late stages of apoptosis, marked by crescent-shaped or granular green staining, were observed after the treatment with NPs systems in the experimental groups. It is noteworthy that in experimental groups, staining was localized asymmetrically within the cells, whereas in normal cells, it was symmetrically deployed. To examine the mechanisms of action of the tested NPs in HeLa cells in greater detail, the cell cycle distribution was determined.

As shown in Fig. 7, 24 hours after exposure to nanoparticles, the number of HeLa cells in the G1 phase increased moderately for all tested compounds. Also, sub-G1 fraction increased for cells treated with any of the studied nanoparticles. The accumulation of cells in the G1 phase and the increased number of cells in the sub-G1 phase is accompanied with a decrease in the proportion of cells in the G2/M and S phases, compared to the control, untreated HeLa cells. Apoptosis in HeLa cells was confirmed, and the distribution of the cell cycle was homogeneous, which was not the case when compounds **A**, **B** and **C** were free.

During the testing of the pure hybrids (**A**, **B** and **C**), apoptosis was also confirmed, but the distribution of the cell cycle was non-homogeneous, confirming that the presence of the drug carrier did not only contribute to the activity and
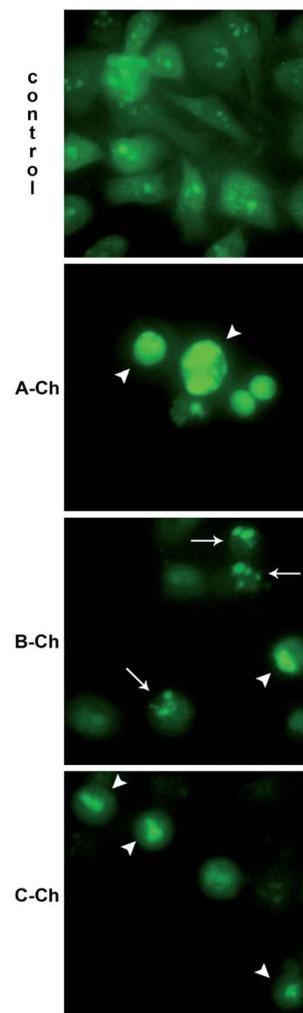

Fig. 6 Control – negative control group (normal cells): circular nuclei are uniformly distributed in the cells. Images **A**-Ch, **B**-Ch, **C**-Ch show experimental groups (apoptotic cells) after the treatment with the corresponding NPs. Green fluorescence from acridine orange staining, which is present in crescent-like or granular form, can be observed in the nuclei. Arrows indicate apoptotic cells with fragmented nuclei, while arrowheads mark cells with condensed chromatin.

selectivity of Biginelli hybrids, but it also significantly affected the cell cycle.

Experimental

Synthesis of A, B and C

To 1.5 mmol of *N*-methylurea in a 5 mL round-bottom flask, a mixture of ethyl-4-chloroacetoacetate (1 mmol) and aldehyde (1 mmol of vanillin, *p*-benzyloxybenzaldehyde, and 5-iodo-vanillin for synthesis of **A**, **B** and **C**, respectively) was added and after that, 0.5 g PEG-1000 and two drops of HCl (36.5%) were added at 70 °C. Two hours later, a 70% ethanol–water solution (10 mL) was added into the reaction mixture and boiled for 0.5 h. After cooling in a refrigerator, the desired products were crystalized, filtrated, and washed with a cooled 70% ethanol–water solution.
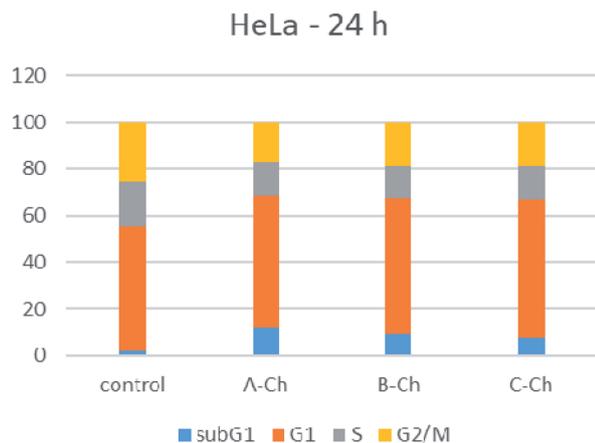
Fig. 7 Cell cycle distribution after 24 h, continuous action of investigated NPs (A-Ch, B-Ch and C-Ch). After exposure for 24 h (the concentration corresponded to the IC_{50} value obtained in the MTT test), cells were harvested, stained with propidium iodide.

Synthesis of A-loaded Ch (A-Ch), B-loaded Ch (B-Ch) and C-loaded Ch (C-Ch)

Chitosan (Ch) with a medium molecular weight (Sigma-Aldrich, deacetylation > 80%), dissolved in acetic acid (1 wt%), was mixed with an ethanol solution of **A** (**B** or **C**) in the Ch : **A** (**B** or **C**) = 8 : 2 weight ratio, while stirring with a magnetic stirrer at 400 rpm. The obtained mixture of **A** (or **B** or **C**), and Ch was slowly poured into a sodium triphosphate pentabasic solution (STP, Sigma-Aldrich) 0.1 wt% in H_2O, while stirring at 21 000 rpm for 30 min. The obtained mixture was then centrifuged at 5000 rpm and 5 °C for 1 h, and the resulting precipitate was subjected to lyophilization at temperatures ranging from −10 to −60 °C and pressures ranging from 0.37 mbar to 0.1 mbar for 1 h to 8 h. The obtained powder was washed with distilled water three times, centrifuged at 1000 rpm and dried again. The final products were powders composed of **A**-Ch, **B**-Ch and **C**-Ch particles.

Characterization of the products

The NMR spectra of the compounds **A**–**C** (ESI, Fig. S1–S6†) were recorded in $CDCl_3$ or DMSO-d_6, with TMS as the internal standard on a Varian Gemini 200 MHz NMR spectrometer (^{1}H at 200 and ^{13}C at 50 MHz). Fourier transform infrared spectroscopy (FT-IR) was performed on a Nicolet iS10 FT-IR Spectrometer equipped with an attenuated total reflectance (ATR) accessory in the spectral range from 400 to 4000 cm^{-1}.

Thermogravimetric and differential thermal analysis (TG-DTA) was performed on a simultaneous TG-DTA (Setsys, SETARAM Instrumentation, Caluire, France) coupled with a mass spectrometric (MS) gas analyzer (Omni Star, Pfeiffer). About 10 mg of the samples were analyzed in the 28–700 °C temperature range under the air flow of 20 mL min^{-1}, in an Al_2O_3 pan. The heating profile was set as follows: the material was stabilized at 28 °C for 5 min, and then heated to 700 °C with the heating rate of 10° min^{-1}.

Field Emission Scanning Electron Microscopy (FE-SEM) was performed on a Carl Zeiss ULTRA Plus microscope at the electron acceleration voltage of 3 kV.

Drug release

High-performance liquid chromatography (HPLC) was applied to measure the encapsulation efficiency of the Biginelli hybrids (**A**, **B** and **C**) and the *in vitro* drug release profile. Solutions of all three systems were prepared in PBS in a concentration of 1 mg mL^{-1} and in the presence of 0.1 wt% sodium lauryl sulfate (SLS). To estimate the release of pure **A**, **B** or **C** at different time points, all measurements were carried out in triplicate at 37 °C. An Agilent 1100 Series system with a diode array detector was used for the analysis and ZORBAX Rx-SIL (4.6 mm × 250 mm, 5 μm) column was employed for separation. The mobile phase consisted of water and acetonitrile and the estimated flow rate was 0.5 mL min^{-1}. Gradient elution was performed in the following way: 0–5 min with 20% of the acetonitrile, 5–25 min 20–100% gradient of the acetonitrile. The detection of pure products was performed using a UV detector at the wavelength of 254 nm.

The concentrations of free **A**, **B** and **C** were calculated using the equation:

$$C_{THPM} (\%) = [(A_{THPM} \times V_{standard} \times C_{standard})/(A_{standard} \times V_{THPM} \times C_{THPM})] \times 100$$

A_{THPM} and $A_{standard}$ (mAU × min) is the area of the released THPM (**A**, **B** or **C**) and standard (pure **A**, **B** or **C** which serve as standard) in HPLC chromatograms, V_{THPM} and $V_{standard}$ are the injection volumes of **A**, **B** or **C** and standard solutions, respectively, and C_{THPM} and $C_{standard}$ are the concentrations of **A**, **B** or **C** and the standard solutions, respectively.

Drug entrapment efficiency

The nanoparticulate formulation systems were suspended in PBS in a concentration of 1 mg mL^{-1} each and kept for 24 h at room temperature. After 24 h solutions were stirred for 5 min and filtered. The encapsulation efficiency of the formulated NPs was measured spectrophotometrically at 254 nm using a Shimadzu UV spectrophotometer. The values were calculated in percentages using the following equation:

$$\text{Percentage of drug entrapment efficiency} = (\text{actual drug content}/\text{theoretical drug content}) \times 100$$

Loose surface crystal study (LSC)

In order to estimate the amount of drug present on the surface of NPs and amount instantly released upon suspension of NPs in the dissolution media, a loose surface crystal study was performed. Suspension solutions of the three NPs systems were prepared in a concentration of 1 mg mL^{-1} and then shaken for 15 minutes vigorously. The amount of drug released from the surface was measured spectrophotometrically at 254 nm. The

LSC values were calculated as the percentage of drug released with respect to entrapped drug.

Cell cultures

The cytotoxicity studies of the three nanoparticulate systems were performed using four cell lines: human cervix adenocarcinoma (HeLa ATCC CCL-2) human colorectal adenocarcinoma, (LS-174 ATCC CL-188), human lung carcinoma (A549 ATCC CCL-185) and normal human lung fibroblasts (MRC-5 ATCC CCL-171). Cells were grown to confluence in a nutrient medium (RPMI-1640 without phenol red) supplemented with 3 mM L-glutamine, 100 µg mL^{-1} streptomycin, 100 IU mL^{-1} penicillin, 10% heat inactivated fetal bovine serum (FBS), and 25 mM Hepes, adjusted to pH 7.2 by a bicarbonate solution. RPMI-1640, FBS, Hepes, and L-glutamine were products of Sigma Chemical Co., St. Louis, MO. Cell cultures were maintained under standard conditions: at a temperature of 37 °C, in in humidified air atmosphere with 5% CO$_2$ and were passaged twice a week. For the experiments, cells between the third and tenth passages were used.

MTT assay

Cell viability was investigated using a MTT assay. Stock solutions of the NPs (10 mg mL^{-1} of active constituent) and pure Biginelli pyrimidines (20 mg mL^{-1}), were prepared in DMSO and then dissolved in a corresponding medium to achieve adequate working concentrations. The final concentration of the DMSO solvent never exceeded 0.5%, a concentration considered non-toxic to the cells. HeLa (2500 cells per well), LS-174 (7000 cells per well), A549 (5000 cells per well), and MRC-5 (5000 cells per well) were seeded into 96-well microtiter plates. Twenty hours later, after the cell adherence, five different concentrations of the investigated compounds in a complete nutrient medium were added to the wells, except for the control cells, to which only the nutrient medium was added. Cell survival was determined by a MTT test according to the method of Mosmann,[37] as modified by Ohno and Abe,[38] 72 h after the addition of the drug. Briefly, 20 µL of MTT solution [3-(4,5-dimethylthiazol-2-yl)-2,5-diphenyltetrazolium bromide, 5 mg mL^{-1} in phosphate buffered saline] was added to each well. The samples were incubated for further four hours at 37 °C in humidified atmosphere with 5% CO$_2$. Then, 100 µL of 10% SDS was added to the wells. Absorbance was measured at 570 nm the following day on a microtiter plate reader (Multiscan Ascent, Thermo Labsystems). To calculate cell survival, absorbance at 570 nm of the sample with the cells grown in the presence of various concentrations of nanoparticles was divided with the absorbance of the control sample (the absorbance of cells grown only in the nutrient medium), implying that the absorbance of the blank was always subtracted from the absorbance of the corresponding sample with the target cells.

Morphological analysis of HeLa cells death

In order to determine the mode of the HeLa cell death induced by the investigated compounds, a morphological analysis using the microscopic examination of acridine orange and ethidium bromide stained cells was performed. HeLa cells were seeded overnight on coverslips (5 × 10^4 cells) in 3 mL of the complete medium, and on the following day, they were treated with the investigated compounds for 24 h. The concentrations applied corresponded to double IC$_{50}$ concentrations of the investigated NPs. The cells were subsequently stained with 6 µL of DNA dyes acridine orange and ethidium bromide (3 mg mL^{-1} AO and 10 mg mL^{-1} EB in 2% solution of ethanol in water) and visualized under a fluorescence microscope using a fluorescein isothiocyanate (FITC) filter set. Typically, the morphological features of the apoptotic cells were highly condensed and/or fragmented nuclei stained with DNA dyes. In the first phase of late apoptosis only acridine orange entered the cell but ethidium bromide was excluded, and the nucleus was stained green. In the second phase of late apoptosis, along with the loss of membrane integrity, both dyes entered the cell and the nucleus became orange-red.

Cell cycle determination

Aliquots of 5 × 10^5 control or the cells treated with NPs for 24 h were fixed in 70% ethanol on ice for one week and centrifuged. The applied concentrations of NPs corresponded to the IC$_{50}$ values obtained in the MTT test after incubation for 72 h. The pellet was treated with RNase A (100 µg mL^{-1}) at 37 °C for 30 min and then incubated with 40 µg mL^{-1} propidium iodide (PI) for at least 30 min. The cells were analyzed using a FACS-Calibur flow cytometer (BD Biosciences Franklin Lakes, NJ, USA) equipped with a 15 mW, air-cooled 488 nm argon ion laser for the excitation of PI. PI fluorescence (FL2) was collected after passing a 585/42 nm band pass filter. The FACSCalibur flow cytometer was equipped with an FL2 upgraded doublet discrimination module (DDM), which allows to screen and then exclude possible occurrences of cell doublets, clumps and debris by plotting FL2-area versus FL2-width signals,[39] PI fluorescence data were collected using linear amplification. A minimum of 10 000 events were collected on each sample. Finally, data were analyzed using the FlowJo™ Software (for Windows, Version 10.3. Ashland, OR: Becton, Dickinson and Company; 2019).

Statistical analysis

Results are expressed as the mean ± standard deviation. All experiments were performed in triplicate and the data were calculated by Student's t-test.

Conclusions

We hereby report the synthesis of chitosan-based nanoparticles and their use as a carrier for selected Biginelli-based anticancer compounds (THPMs). THPMs (A, B and C) were synthesized and introduced for the first time into the vehicles made of chitosan (Ch). During the SEM analysis, two types of particles were registered in the investigated systems, larger – with an average diameter of 100 ± 20 nm, and smaller – with an average diameter of 30 ± 10 nm. The selectivity of the prepared NPs was

examined using the MTT test in HeLa, LS-174, A549, MRC-5. The obtained results indicate that all nanoparticulate systems (**A**-Ch, **B**-Ch, and **C**-Ch) exhibit significantly greater cytotoxicity to the selected cancer cell lines than THPMs (**A**, **B**, and **C**). On the other hand, the toxicity to healthy cell lines is significantly diminished compared to that of pure compounds. Therefore, after the treatment of HeLa cells with NPs systems during a period of 24 hours, an early apoptosis was recorded. In general, after the treatment with NPs, the distribution of the cell cycle was homogeneously affected. As far as the drug release process is concerned, it can be observed that almost total drug amount was released in three days, which suggest that the prepared system enables relatively fast drug delivery. We have designed a carrier suitable for the delivery of the Biginelli-based drugs with a multifunctional effect: it allows selectivity and has an improved anticancer activity followed by homogeneous cell cycle distribution.

Conflicts of interest

There are no conflicts to declare.

Acknowledgements

Notes and references

1 C. O. Kappe, *Eur. J. Med. Chem.*, 2000, **35**, 1043–1052.

2 C. O. Kappe, *Tetrahedron*, 1993, **49**, 6937–6963.

3 K. S. Atwal, B. N. Swanson, S. E. Unger, D. M. Floyd, S. Moreland, A. Hedberg and B. C. O'Reilly, *J. Med. Chem.*, 1991, **34**, 806–811.

4 T. U. Mayer, T. M. Kapoor, S. J. Haggarty, R. W. King, S. L. Schreiber and T. J. Mitchison, *Science*, 1999, **286**, 971–974.

5 A. Pawar and P. Prabhu, *Biomed. Pharmacother.*, 2019, **110**, 319–341.

6 A. Basu, P. Upadhyay, A. Ghosh, D. Chattopadhyay and A. Adhikary, *ACS Biomater. Sci. Eng.*, 2019, **5**, 373–389.

7 O. Tacar, P. Sriamornsak and C. R. Dass, *J. Pharm. Pharmacol.*, 2013, **65**, 157–170.

8 S. Sarkar, S. Konar, P. N. Prasad, S. Rajput, B. N. P. Kumar, R. R. Rao, A. Pathak, P. B. Fisher and M. Mandal, *Langmuir*, 2017, **33**, 7649–7659.

9 O. C. Farokhzad and R. Langer, *ACS Nano*, 2009, **3**(1), 16–20.

10 G. De Crozals, R. Bonnet, C. Farre and C. Chaix, *Nano Today*, 2016, **11**, 435–463.

11 C. Alvarez-Lorenzo, A. Rey-Rico, A. Sosnik, P. Taboada and A. Concheiro, *Front. Biosci.*, 2010, **2**, 424–440.

12 K. Hayashi, Y. Sato, H. Maruoka, W. Sakamoto and T. Yogo, *ACS Biomater. Sci. Eng.*, 2017, **3**(6), 1129–1135.

13 R. A. Petros and J. M. DeSimone, *Nat. Rev. Drug Discovery*, 2010, **9**(8), 615–627.

14 L. Bugnicourt and C. Ladaviere, *Prog. Polym. Sci.*, 2016, **60**, 1–17.

15 K. Zhao, Y. Zhang, X. Zhang, C. Shi, X. Wang, X. Wang, Z. Jin and S. Cui, *Int. J. Nanomed.*, 2014, **9**, 4609–4619.

16 M. Prabaharan and J. F. Mano, *Drug Deliv.*, 2005, **12**, 41–57.

17 P. Sanpui, A. Murugadoss, P. V. Prasad, S. S. Ghosh and A. Chattopadhyay, *Int. J. Food Microbiol.*, 2008, **124**, 142–146.

18 N. L. Ignjatović, M. Sakač, I. Kuzminac, V. Kojić, S. Marković, D. Vasiljević-Radović, V. Wu, V. Uskoković and D. P. Uskoković, *J. Mater. Chem. B*, 2018, **6**, 6957–6968.

19 N. L. Ignjatović, K. M. Penov-Gaši, J. J. Ajduković, V. V. Kojić, S. B. Marković and D. P. Uskoković, *Mater. Sci. Eng. C*, 2018, **89**, 371–377.

20 N. L. Ignjatović, K. M. Penov-Gaši, V. Wu, J. J. Ajduković, V. V. Kojić, D. Vasiljević-Radović, M. Kuzmanović, V. Uskoković and D. P. Uskoković, *Colloids Surf., B*, 2016, **148**, 629–639.

21 N. Janković, J. Trifunović Ristovski, M. Vraneš, A. Tot, J. Petronijević, N. Joksimović, T. Stanojković, M. Đorđić Crnogorac, N. Petrović, I. Boljević, I. Z. Matić, G. A. Bogdanović, M. Mikov and Z. Bugarčić, *Bioorg. Chem.*, 2019, **86**, 569–582.

22 J. Petronijević, Z. Bugarčić, G. A. Bogdanović, S. Stefanović and N. Janković, *Green Chem.*, 2017, **19**, 707–715.

23 M. Gavrilović, N. Janković, Lj. Joksović, J. Petronijević, n. Joksimović N and Z. Bugarčić, *Environ. Chem. Lett.*, 2018, **16**, 1501–1506.

24 N. Janković, S. Stefanović, J. Petronijević, N. Joksimović, S. B. Novaković, G. A. Bogdanović, J. Muškinja, M. Vraneš, Z. Ratković and Z. Bugarčić, *ACS Sustainable Chem. Eng.*, 2018, **6**, 13358–13366.

25 M. Vranes, J. Panić, A. Tot, S. Ostojic, D. Četojević-Simin, N. Janković and S. Gadzuric, *ACS Sustainable Chem. Eng.*, 2019, **7**, 10773–10783.

26 N. Janković, Z. Bugarčić and S. Marković, *J. Serb. Chem. Soc.*, 2015, **80**, 595–604.

27 J. Muškinja, N. Janković, Z. Ratković, G. Bogdanović and Z. Bugarčić, *Mol. Divers.*, 2016, **20**, 591–604.

28 S. N. Tammam, H. M. E. Azzazy, H. G. Breitinger and A. Lamprecht, *Mol. Pharm.*, 2015, **12**, 4277–4289.

29 H. Seifi, T. Gholami, S. Seifi, S. M. Ghoreishi and M. Salavati-Niasari, *J. Anal. Appl. Pyrol.*, 2020, **149**, 104840.

30 T. Wanjun, W. Cunxin and C. Donghua, *Polym. Degrad. Stab.*, 2005, **87**, 389–394.

31 K. A. Milligan, C. Winstead and J. Smith, *Int. J. Pharm. Sci. Res.*, 2018, **9**(4), 1430–1440.

32 H. Thai, C. Thuy Nguyen, L. Thi Thach, M. Thi Tran, H. Duc Mai, T. Thi Thu Nguyen, G. Duc Le, M. Van Can, L. Dai Tran, G. Long Bach, K. Ramadass, C. I. Sathish and Q. Van Le, *Sci. Rep.*, 2020, **10**, 909.

33 M. Stevanovic, N. Ignjatovic, B. Jordovic and D. Uskokovic, *J. Mater. Sci.: Mater. Med.*, 2007, **18**, 1339–1344.

34 Y. S. Cho, G. R. Yi, S. H. Kim, M. T. Elsesser, D. R. Breed and S. M. Yang, *J. Colloid Interface Sci.*, 2008, **318**, 124–133.

35 F. Khakzad, A. R. Mahdavian, H. Salehi-Mobarakeh and M. H. Sharifian, *J. Colloid Interface Sci.*, 2018, **515**, 58–69.

36 E. P. Pedraza and M. D. Soucek, *Eur. Polym. J.*, 2007, **43**, 1530–1540.

37 T. Mosmann, *J. Immunol. Methods*, 1983, **65**, 55–63.

38 M. Ohno and T. Abe, *J. Immunol. Methods*, 1991, **145**, 199–203.

39 M. Carbonari, T. Tedesco and M. Fiorilli, *Cytometry*, 2001, **44**, 120–125.